Low-lying states in ^{32}Mg studied by proton inelastic scattering

S. Takeuchi,[1,*] N. Aoi,[1] T. Motobayashi,[1] S. Ota,[2,†] E. Takeshita,[3,‡] H. Suzuki,[4,‡] H. Baba,[1] T. Fukui,[2] Y. Hashimoto,[5] K. Ieki,[3] N. Imai,[6] H. Iwasaki,[4] S. Kanno,[3,‡] Y. Kondo,[5,‡] T. Kubo,[1] K. Kurita,[3] T. Minemura,[6,§] T. Nakabayashi,[5] T. Nakamura,[5] T. Okumura,[5] T. K. Onishi,[4] H. Sakurai,[4,‡] S. Shimoura,[7] R. Sugou,[3] D. Suzuki,[4] M. K. Suzuki,[4] M. Takashina,[8] M. Tamaki,[7] K. Tanaka,[1] Y. Togano,[3,‡] and K. Yamada[1]

[1]*RIKEN Nishina Center, 2-1 Hirosawa, Wako, Saitama 351-0198, Japan*
[2]*Department of Physics, Kyoto University, Kitashirakawa, Kyoto 606-8502, Japan*
[3]*Department of Physics, Rikkyo University, 3-34-1 Nishi-Ikebukuro, Toshima, Tokyo 172-8501, Japan*
[4]*Department of Physics, University of Tokyo, 7-3-1 Hongo, Bunkyo, Tokyo 113-0033, Japan*
[5]*Department of Physics, Tokyo Institute of Technology, 2-12-1 Ookayama, Meguro, Tokyo 152-8551, Japan*
[6]*Institute of Particle and Nuclear Study, KEK, 1-1 Oho, Tsukuba 305-0801, Japan*
[7]*Center for Nuclear Study, University of Tokyo, RIKEN Campus, 2-1 Hirosawa, Wako, Saitama 351-0198, Japan*
[8]*Research Center for Nuclear Physics (RCNP), Osaka University, Ibaraki, Osaka 567-0047, Japan*

(Received 15 April 2009; published 15 May 2009)

Proton inelastic scattering on the neutron-rich nucleus ^{32}Mg has been studied at 46.5 MeV/nucleon in inverse kinematics. Populated states were identified by measuring de-excitation γ rays, in which five new states were found by γ-γ coincidence analyses. By analyzing the angular differential cross sections via coupled-channel calculations, their spins and parities were constrained and the amplitudes for each transition were extracted. The spin and parity of the 2321-keV state was assigned as 4^+_1. The ratio between the energies of the 2^+_1 and 4^+_1 states indicates that ^{32}Mg is a transitional nucleus rather than an axially deformed rigid rotor. The collectivities in the nucleus ^{32}Mg with $N = 20$ are discussed based on the results obtained in the present experiment.

DOI: 10.1103/PhysRevC.79.054319 PACS number(s): 23.20.Lv, 23.20.En, 25.60.−t, 25.40.Ep

I. INTRODUCTION

The nucleus ^{32}Mg in the island of inversion [1] has drawn much interest because of its anomalously large quadrupole collectivity [2,3] in spite of its neutron number $N = 20$ being magic in traditional nuclear theory. One piece of evidence for the anomaly is the large $B(E2; 0^+_{\text{g.s.}} \rightarrow 2^+_1)$ value extracted by the Coulomb excitation measurements for ^{32}Mg [3–8]. The first measurement was performed by Motobayashi *et al.* [3], who reported the value of $B(E2) = 454(78)\,e^2$ fm^4 corresponding to a large deformation of $\beta_2^{\text{em}} = 0.512(44)$. This value supports the large collectivity suggested by the low excitation energy of the first 2^+ state [$E_x(2^+_1) = 885$ keV] [2] and points to the vanishing of the $N = 20$ shell gap. This finding has shown that the nuclear shell structure can change in the region far from the stability line and has triggered many experimental and theoretical works focusing on the evolution of shell structure in a wide range of nuclei. Indeed, the disappearances of the magic numbers $N = 8$ [9–12] and $N = 28$ [13,14], as well as the appearance of the new magic number $N = 16$ [15], have been found in the succeeding studies.

Theoretically, the large $B(E2)$ value and the small $E_x(2^+_1)$ value were interpreted using shell-model calculations by introducing the neutron 2p-2h excitation across the *sd*-*pf* shell gap, suggesting a breaking of the $N = 20$ shell closure [16–21]. Mean-field calculations result in a spherical shape for the ground state [22,23]. However, it is calculated to be very soft against quadrupole deformation. The low-lying 2^+_1 state is reproduced by the quasiparticle random-phase approximation [24] and configuration mixing with angular-momentum projection [25,26].

Beyond the 2^+_1 state, the nature of 3^-_1 and 4^+_1 states is particularly crucial in understanding quantitatively the anomaly in the $N = 20$ shell gap and the character of collectivity in this nucleus. The location of the 3^-_1 state reflects the size of the $d_{3/2}$-$f_{7/2}$ shell gap, if the state is of single-particle character or the transition strength is close to the single-particle value. The ratio between the energies of the 2^+_1 and 4^+_1 states gives information on the nature of quadrupole collectivity. However, experimental information is rather limited in terms of the excitation energies and firm spin and parity (J^π) assignments of the low-lying states, except for 2^+_1.

Attempts to search for states above 2^+_1 in ^{32}Mg have so far been done by using β decays, fragmentation reactions, nuclear inelastic scattering, and Coulomb excitation reactions. An excited state at $E_x = 2321$ keV provides a potential candidate for either the 3^- or 4^+ state [27,28]. In the β decay of ^{32}Na [28], the 2321-keV state is not directly populated, leading to a positive-parity assignment to this state. The authors of Ref. [28] argue that it is the most likely candidate for the 4^+_1 state. This 4^+_1 assignment is consistent with the quadrupole character of the γ transition from the 2321-keV state to the 2^+_1 state studied by the γ-γ angular correlation in the fragmentation reaction of ^{36}S [29,30]. However, a 3^- assignment for the 2321-keV state was proposed in a nuclear inelastic scattering experiment by considering the similarity between the observed cross section and that for

*takesato@riken.jp
†Present address: Center for Nuclear Study, University of Tokyo.
‡Present address: RIKEN Nishina Center.
§Present address: National Cancer Center, 5-1-1 Tsukiji, Chuo, Tokyo 104-0045, Japan.

the 3^- state in ^{34}Si [27]. Other J^π assignments of 1^-, 1^+, and 2^+ were suggested in an intermediate-energy Coulomb excitation study [4]. Other excited states in ^{32}Mg have been observed by β-decay experiments to construct the level scheme [2,28,31–33]. However, definitive J^π assignments to these states have not yet been made. The present article reports on a study of low-lying levels in ^{32}Mg by measuring proton inelastic scattering.

Proton inelastic scattering populates a variety of excited states with different characters and have been extensively used for the study of stable nuclei. Angular distributions of differential cross sections reflect the transferred angular momentum (ΔL). Therefore, J^π values of the relevant states are determined or constrained by analyses of angular distributions with appropriate reaction theories such as the distorted-wave Born approximation. The amount of nuclear collectivity, often expressed by a parameter called deformation length, can be studied from the amplitude of the cross section. Moreover, the proton and neutron collectivity can be studied separately by comparing the deformation length extracted from the cross section of proton inelastic scattering with the one extracted from the $B(E2)$ value obtained via Coulomb excitation or lifetime measurements [34,35].

In-beam measurement of γ rays associated with intermediate-energy proton inelastic scattering is suitable for studying low-lying excited states in unstable nuclei that are produced as low-intensity beams [10,36–41]. Since excitation energies are determined by measuring de-excitation γ rays, thick targets can be used, which enables highly efficient measurements as compared with the missing-mass method, where thinner targets are used to measure low-energy recoil protons [42–46]. The efficiency is particularly high when a liquid-hydrogen target is used, owing to the large number of target atoms available for a given areal density. Consequently, measurements by beams of very neutron rich nuclei with extremely low intensity become possible, as demonstrated in the studies of ^{30}Ne [36], ^{27}F [41], ^{40}Si [39,47], and ^{62}Cr [40].

In the experiment described in the present article, de-excitation γ rays from ^{32}Mg and the scattered ^{32}Mg nuclei were measured in coincidence. Doppler-shifted γ rays were measured by a high-efficiency γ-ray detector array with sensitivity to the γ-ray emission angle. The γ-γ correlations were analyzed to construct the level scheme, and the angular distributions of the inelastically scattered ^{32}Mg nuclei were analyzed by the distorted-wave calculations to deduce ΔL for each excitation, leading to the J^π assignments. As a result, several new levels have been identified and spin assignments have been made for a few states including the one at $E_x = 2321$ keV. The extracted deformation length in the 2_1^+ excitation was used to discuss the neutron and proton contributions by comparing with the result from the Coulomb excitation experiment.

In addition to inelastic scattering, the two-neutron removal reaction was studied simultaneously by measuring de-excitation γ rays from ^{30}Mg in coincidence with ^{30}Mg nuclei. A candidate of the transition from the 4^+ state in ^{30}Mg was found in the observed γ-ray spectrum, providing useful information for systematic study of the collectivity in Mg isotopes.

II. EXPERIMENT

The experiment was performed at the RI Beam Factory operated by RIKEN Nishina Center and Center for Nuclear Study, University of Tokyo. A primary ^{40}Ar beam of 94 MeV/nucleon provided by the $K = 540$ MeV ring cyclotron bombarded a ^{9}Be production target of thickness 370 mg/cm^2. Various products of projectile fragmentation reactions were analyzed using the RIKEN projectile fragment separator (RIPS) [48] to obtain a radioactive ^{32}Mg beam. To identify the ^{32}Mg ions in the secondary beam, the time of flight (TOF) and the energy loss (ΔE) were measured on an event-by-event basis by two plastic scintillators set at the second and third foci (F2 and F3) and a silicon detector located at F3, respectively. The energy and intensity of the ^{32}Mg beam were 56 MeV/nucleon and 450 particles per second, respectively. The fraction of ^{32}Mg in the secondary beam was about 15%. The incident angle of the incoming ^{32}Mg nucleus was measured on an event-by-event basis by two position-sensitive parallel-plate avalanche counters (PPACs) [49] set 87 cm apart from each other located at around the F3 focus, as shown in Fig. 1.

The ^{32}Mg beam bombarded a liquid-hydrogen target [50] located at the exit of RIPS. We employed the target system CRYPTA (CRYogenic ProTon and Alpha target system), which consisted of a target cell filled with liquid hydrogen and a cryogenic refrigerator. The target cell was of cylindrical geometry with a diameter of 3 cm; the entrance and exit windows consist of 7-μm-thick Havar foils. Hydrogen gas was cooled to 16 K under a pressure of around 0.1 MPa by a cryogenic refrigerator to be liquefied. The average thickness of hydrogen was 157 mg/cm^2. The average energy of the ^{32}Mg beam in the target was estimated to be 46.5 MeV/nucleon.

Scattered particles were analyzed by the spectrometer TOMBEE (TOf Mass analyzer for exotic BEam Experiment)

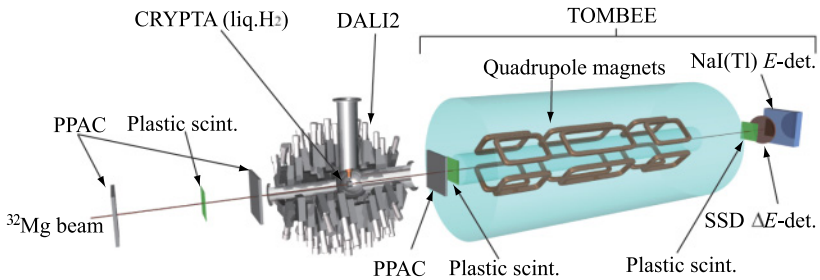

FIG. 1. (Color online) Illustration of the present experimental setup with focal-plane detectors at F3 of RIPS, CRYPTA, DALI2, and TOMBEE.

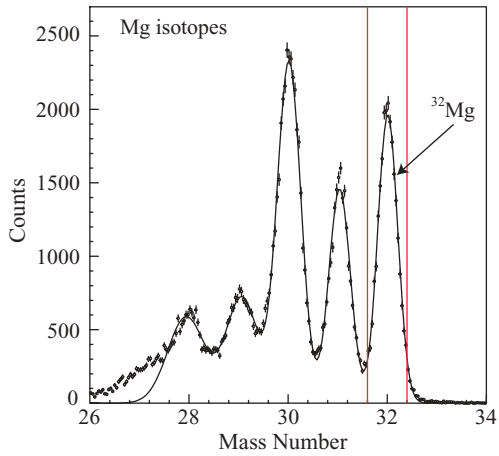

FIG. 2. (Color online) Experimental mass distribution for Mg isotopes obtained using the TOMBEE spectrometer. The solid curve shows the result of a fit using Gaussian functions. The red lines indicate the region of the mass gate used in the analysis.

[51], which was placed 0.9 m downstream of the reaction target. TOMBEE consists of several detectors and superconducting triplet quadrupole (STQ) magnets [52]. Scattered particles were delivered to the focus of TOMBEE by the STQ magnets. At the focus, a plastic scintillator (0.5 mm thick), a silicon detector (134 mm in diameter and 320 μm thick), and an array of NaI(Tl) scintillators (5 cm thick arranged in a 6×6 matrix) [53] were set for precise particle identification. Another plastic scintillator was positioned 50 cm downstream of the reaction target to form a 4-m flight path for the TOF measurement with the one at the focus of TOMBEE. Energy loss (ΔE) and total kinetic energy (E) of a scattered particle were measured by the silicon detector and the array of NaI(Tl) scintillators, respectively. The atomic number and the mass number of each particle were determined by utilizing the ΔE-TOF and E-TOF methods, respectively. Figure 2 shows the mass distribution for the Mg isotopes. The obtained mass resolution was around 1.5% in full width at half maximum (FWHM), which is considerably better than the 2.5% (FWHM) resolution obtained in the earlier experiments [36,41,54] using the ΔE-E method with silicon detectors. With this high mass resolution, contaminants in the ^{32}Mg mass gate set in the present analysis (indicated by the red lines in Fig. 2) were as low as 1%. The scattering angles of the relevant inelastic scattering products were obtained from the incident and outgoing angles measured by PPACs placed upstream and downstream of the reaction target. The typical resolution of the scattering angle in the laboratory system was estimated to be $0.23^\circ(1\sigma)$, including multiple scattering (0.17°) in the reaction target. The transmission of TOMBEE was measured to be about 95% at 0° and 50% at 2.5°, respectively, by using scattered ^{32}Mg.

De-excitation γ rays were detected by using the DALI2 (Detector Array for Low-Intensity radiation 2) array [55], which consisted of 160 NaI(Tl) crystals surrounding the reaction target. Each scintillator has a rectangular shape with dimensions of $40 \times 80 \times 160$ mm, coupled to a 38-mm-ϕ photomultiplier tube. Sixteen layers, each of which consisted of 6–14 scintillators, were set perpendicular to the beam axis, covering the angular range of 20°–160°. The distance from the target to the center of each scintillator was about 30 cm for the layer around 90°. Each detector is supported by a 3-mm-thick aluminum plate, which are mounted at 5-cm intervals. An energy calibration was performed with standard ^{22}Na, ^{60}Co, and ^{137}Cs sources. The uncertainty of energy determinations in the energy region above $E_\gamma = 1.3$ MeV (^{60}Co source) was estimated to be 0.5% by comparing with the 2.6-MeV γ-ray peak observed in a natural-background measurement. The full-energy-peak efficiency and energy resolution were obtained to be about 24% and 9% (FWHM), respectively, at 662 keV (^{137}Cs). In this study, the γ rays were emitted from fast-moving nuclei with a velocity of $v/c \simeq 0.3$, which causes a considerable Doppler shift in the observed γ-ray energies. The measured γ-ray energy in the laboratory system was converted to the relevant moving frame of reference by using the γ-ray emission angle. The angular resolution of γ-ray detection is about 7° at γ-ray emission angles of 70°, where the Doppler-shift effect is largest.

In the data analyses, the response (i.e., the energy spectrum expected for monoenergetic γ rays from a moving source) of the DALI2 system to the γ ray of interest was used to extract the γ-ray yield from the measured γ-ray spectrum. It was obtained by Monte Carlo simulations by taking into account the energy resolution of each detector and the geometry of the NaI(Tl) detectors, the target cell, and the target chamber using the GEANT3 code [56]. To enhance the full-energy-peak efficiency, an add-back analysis was performed. When two or more adjacent NaI(Tl) crystals were hit, these signals were considered to be generated by one γ-ray scattered or absorbed in a "cluster" of these crystals. The energy of the incident γ ray can be obtained by summing up the energies measured in a given cluster. For the Doppler-shift correction, the γ emission angle was determined by using the angle of the detector with the largest energy deposit in the cluster. With the add-back analysis, the efficiency and energy resolution for 1-MeV γ rays from nuclei with $v/c \simeq 0.3$ were obtained to be 24% and 10% (FWHM), respectively. The systematic error of the simulations was evaluated to be less than 5% by comparison with measurements of γ rays from standard sources.

In the simulations, the nonlinear response of the NaI(Tl) light output was examined, because it is known to be sizable below 400 keV [57,58]. This nonlinearity is caused by the energy dependence of the light yield for electrons moving in a NaI(Tl) crystal. The effect on the add-back analysis was examined by comparing simulations with and without the effect. An extracted shift of about 5 keV was accounted for in evaluating the systematic error.

III. RESULTS

A. γ-ray spectra and level scheme

The γ-ray spectrum associated with $p + ^{32}$Mg inelastic scattering is shown in Fig. 3(a), where Doppler-shift effects are corrected. De-excitation γ rays with $E_\gamma = 887(7)$ keV and $E_\gamma = 1433(9)$ keV are predominant. The γ-ray peak energies were deduced by fits of the spectrum with Gaussian functions and an exponential curve, where the energy resolutions

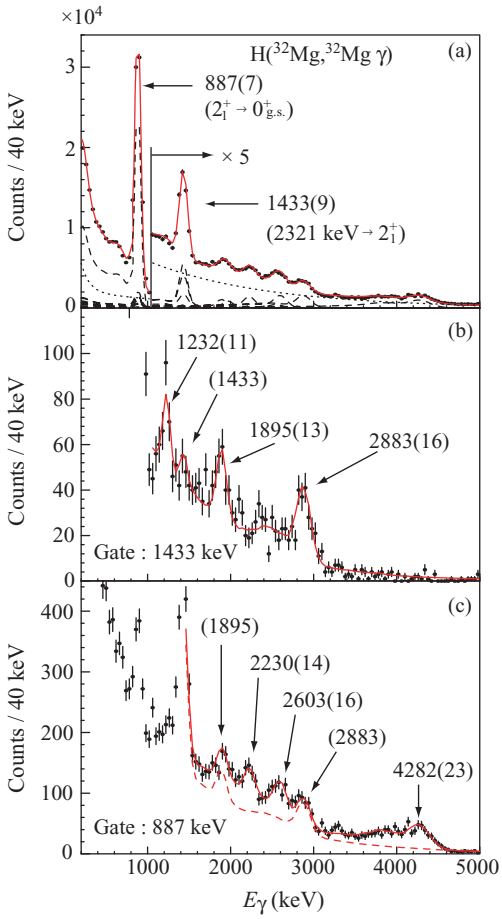

FIG. 3. (Color online) (a) Doppler-corrected γ-ray spectra obtained in the ^{32}Mg(p, p') reaction in inverse kinematics. The red solid curve shows the fitting result using the response functions (dashed curves) and the exponential background (dotted curve). (b) γ-ray spectrum gated on the 1433-keV γ ray, which corresponds to the transition from the 2321-keV state to the 2^+_1 state. The red solid curve shows the result of fitting. (c) γ-ray energy spectrum gated on the 887-keV γ ray, which corresponds to the transition from the 2^+_1 state to the ground state. The red solid curve shows the fitting result. The dashed curve shows the response functions, which correspond to transitions feeding to the 2321-keV state.

were fixed for individual peaks to the simulated values. These two peaks correspond, respectively, to the transition from the 2^+_1 state to the ground state and to the one from the 2321-keV state to the 2^+_1 state. In the spectrum above 1500 keV, several additional peaks are also seen. Some the peaks seen above 1433 keV correspond to new transitions, as these lines were not identified in earlier experiments using Coulomb excitation or nuclear inelastic scattering [3,4,27]. The spectrum was analyzed with response functions obtained through simulations, in which the γ-ray energies were fixed to the values obtained by the Gaussian fits. The energies of the new γ lines are discussed later. The solid curve in Fig. 3(a) shows the result of the fit with the response functions (dashed curves) and an exponential background (dotted curve).

To construct a level scheme, γ-γ coincidence analyses were performed. Figure 3(b) shows the γ-ray spectrum gated on the 1433-keV γ ray peak, which is expected to contain peaks for the transitions feeding the 2321-keV state. Since Compton-scattered events caused by higher energy γ rays decaying to the 2321-keV states are present in the 1433-keV gate, a small peak at 1433 keV is still seen. Three dominant γ lines are observed, as shown in the figure. Their peak energies are 1232(11), 1895(13), and 2883(16) keV, where the errors include the statistical and systematic uncertainties in the energy determination. A fit of the spectrum with the response functions and an exponential background is indicated by the red solid curve in Fig. 3(b). Observation of the 1232-keV peak in the 1433-keV gate supports the assignment given in the most recent β-decay studies [28,33], where the 1232-keV line was proposed to populate the state at 2321 keV. This is in contrast to the population of the 885-keV state, as suggested in Ref. [32]. The quality of the fit is reasonably good, except for the region around 2400 keV, where a moderate buildup of events may indicate the existence of another γ line. However, this "line" is not statistically significant and thus not included in the level scheme, which will be discussed later.

Figure 3(c) shows the γ-ray spectrum gated on the 887-keV γ ray, which corresponds to the $2^+_1 \rightarrow 0^+_{\text{g.s.}}$ transition. New transitions to the 2^+_1 state are found at $E_\gamma =$ 2230(14), 2603(16), and 4282(23) keV. Since the peaks at 1895 and 2883 keV are seen in Fig. 3(b) as well, they should correspond to transitions feeding the 2321-keV state directly. The γ-ray spectrum expected for direct decays to the 2321-keV state is indicated by the dashed curve. In the figure, a peaklike structure is also seen at an energy of 3256(43) keV. However, the corresponding peak with expected yield is missing in the singles γ-ray spectrum [Fig. 3(a)]. Therefore, this γ line is not considered in constructing the level scheme.

Figure 4 shows the level scheme constructed from the results of the γ-γ coincidence analyses just described. The new γ transitions found in this study are shown by the red arrows. Their energies of 1895(13), 2230(14), 2603(16), 2883(16), and 4282(23) keV lead to excitation energies of 4216(13), 3115(14), 3488(16), 5204(16), and 5167(23) keV, respectively, where we adopt the energies of 885 and 2321 keV for the first and second excited states. The J^π values or transferred angular momenta (indicated in parentheses in the figure) are obtained from the analysis discussed in Sec. III B.

The cross sections for exciting the individual states were obtained through fits to the γ-ray spectra and are listed in Table I together with the γ-ray intensities normalized to that of the $2^+_1 \rightarrow 0^+_{\text{g.s.}}$ transition. The errors in the cross sections and the γ-ray intensities include the statistical errors, the uncertainties in the simulations, and uncertainties for the target thickness (=5%). Note that the transitions from the 3037- and 4820-keV states populated by the β decay of ^{32}Na were not observed in the present experiment.

B. Angular distributions of scattered ^{32}Mg and spin assignments

1. The 885- and 2321-keV states

The transferred angular momentum (ΔL) for an inelastic-scattering reaction affects the angular distribution of the scattered particle. In the present case [i.e., ^{32}Mg(p, p')], the

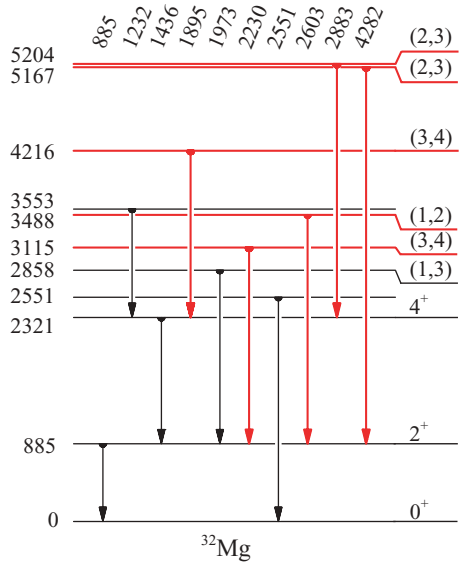

FIG. 4. (Color online) Level scheme for ^{32}Mg deduced in the current study. The red (thick) arrows and lines indicate new transitions and levels. J^π values and transferred angular momenta (in parentheses) are obtained in the present analysis (see Sec. III B for details).

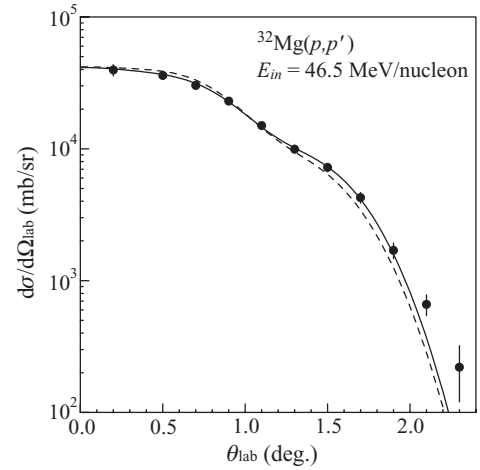

FIG. 5. Angular distribution for the excitation to the 885-keV state in ^{32}Mg indicated by the closed circles. The solid and dashed curves show the coupled-channel calculations with $\Delta L = 2$ excitation assumed within the rotational model.

determination of ΔL imposes a strong constraint on the spin and parity (J^π) of the final state in ^{32}Mg, since the initial J^π is 0^+. In Fig. 5, the experimental angular distribution for the excitation to the 2_1^+ state at 885 keV is indicated by the closed circles. Data were extracted from the γ-ray spectra obtained at different angles for 0.2° or 0.4° bins, where the acceptance of TOMBEE was taken into account. The feeding of the 885-keV state from higher excited states was corrected based on the observed γ-ray spectrum with the help of the level scheme obtained in this study.

TABLE I. Excitation energies, $J^\pi(\Delta L)$, cross sections, and γ-ray intensities observed in the ^{32}Mg(p, p') experiment. Cross sections were obtained by analyses of γ-ray spectra shown in Figs. 3(a), 3(b), and 3(c).

E_x (keV)	$J^\pi(\Delta L)$	σ (mb)	E_γ (keV)	I_γ[a]	E_f[b] (keV)
0	0^+	–	–	–	–
885	2^+	47.6(53)	885	100	0
2321	4^+[c]	3.7(6)	1436	12.3(18)	885
2551	$(1^-, 2^+)$[d]	0.6(3)	2551	1.0(5)	0
2858	$(1, 3)$[e]	0.9(3)	1973	1.4(4)	885
3115	$(3, 4)$[e]	1.7(3)	2230	2.7(5)	885
3488	$(1, 2)$[e]	2.3(5)	2603	3.7(8)	885
3553	$(3^-, 4^-)$[d]	0.3(1)	1232	0.4(2)	2321
4216	$(3, 4)$[e]	1.1(3)	1895	1.7(4)	2321
5167	$(2, 3)$[e]	2.9(4)	4282	4.6(7)	885
5204	$(2, 3)$[e]	2.7(4)	2883	4.3(6)	2321
3037	$(2^-, 3^-)$[d]	–	2152	–	885
4820	$(2^-, 3^-)$[d]	–	3935	–	885
		–	1783	–	3037

[a]Intensities relative to the 885-keV γ ray.
[b]Excitation energy of feeding state.
[c]Assigned in this study.
[d]Taken from Ref. [28].
[e]Tentative assignment of ΔL in this study.

The angular distributions were analyzed by the coupled-channel calculations using the ECIS97 code [59]. In the calculations, two global optical potentials, KD02 [60] and CH89 [61], were employed. The solid and dashed curves in Fig. 5 show the results with $\Delta L = 2$ assumed, which is consistent with the transition from the $0^+_{\text{g.s.}}$ state to the 2_1^+ state in ^{32}Mg, with the rotational model using KD02 and CH89 potentials, respectively. The coupling potential in the ECIS97 calculation is created by the derivative of the optical potential. Note that the calculated curves are convoluted with the angular resolution of 0.23° (1σ) in the laboratory frame. Both calculations reproduce the experimental distribution well, demonstrating the validity of the present coupled-channel analysis with the global optical potential. The best fits for the two optical potentials were obtained with the quadrupole-amplitude parameter or "deformation parameter" $\beta_2 = 0.432(27)$ and 0.479(29), respectively.

For the 2321-keV state, its possible J^π value was suggested to be 3^- from a nuclear inelastic scattering experiment [27] or 4^+ from a β-decay experiment [28], as discussed in Sec. I, but no definitive assignment is given so far. We first examined simple calculations assuming $J^\pi = 0^+$, 1^-, 2^+, 3^-, and 4^+. The amplitude parameters β_λ (where λ denotes multipolarity) that give the best fits are listed in Table II. Figure 6 shows the results with the KD02 potential. The black solid curve shows the distribution for $J^\pi = 0^+$ with a one-phonon excitation ($0^+_{\text{g.s.}} \to 0^+_2$) in the vibrational model (breathing mode) assumed. The black dashed curve indicates another calculation for $J^\pi = 0^+$ in which population via a two-phonon excitation ($0^+_{\text{g.s.}} \to 2^+_1 \to 0^+_2$) is assumed, where the same β_2 values are used for the $0^+_{\text{g.s.}} \to 2^+_1$ and $2^+_1 \to 0^+_2$ excitations. The dot-dashed curve shows the result in which a $J^\pi = 1^-$ one-phonon excitation is assumed. For the $J^\pi = 2^+$

TABLE II. Amplitude and reduced-χ^2 value for each calculation.

J^π	λ	Amplitude (β_λ)	Reduced χ^2
0^+	0	0.082(8)	2.4
	2	0.465(28)	8.2
1^-	1	0.111(11)	2.6
2^+	2	0.464(28)	7.7
3^-	3	0.139(13)	1.9
4^+	2	0.437(27)	6.9
	4	0.153(15)	0.6

case, only the calculation in which a two-step excitation ($0^+_{\text{g.s.}} \rightarrow 2^+_1 \rightarrow 2^+_2$) is assumed is shown in Fig. 6; the transition strengths for the first and second steps are both fixed to the one reproducing the $0^+_{\text{g.s.}} \rightarrow 2^+_1$ excitation. It should be noted that the one-step result, the shape of which is similar to the one shown in Fig. 5 for the $0^+_{\text{g.s.}} \rightarrow 2^+_1$ excitation, does not reproduce the angular distribution for the 2321-keV state.

The blue and red curves show the calculations for $J^\pi = 3^-$ and 4^+, respectively, which are the possible assignments proposed for the 2321-keV state as mentioned before. The distribution for $J^\pi = 3^-$ is calculated by assuming a one-phonon excitation. For $J^\pi = 4^+$, a one-step excitation ($0^+_{\text{g.s.}} \rightarrow 4^+_1$) and a two-step excitation ($0^+_{\text{g.s.}} \rightarrow 2^+_1 \rightarrow 4^+_1$) are assumed within the rotational model. The results are indicated by the solid and dashed red curves, respectively. As seen in Fig. 6, the two-step excitation component, indicated by the red dashed curve, is much smaller than the experimental angular distribution below 1.5° with the same β_2 values (0.437) as for the $0^+_{\text{g.s.}} \rightarrow 2^+_1$ and $2^+_1 \rightarrow 4^+_1$ excitations.

In the experimental angular distribution, the peak around 1.1° is characteristic. The one-step calculation with $J^\pi = 4^+$ reproduces well the peak position as well as the overall shape of the experimental angular distribution, whereas the calculations

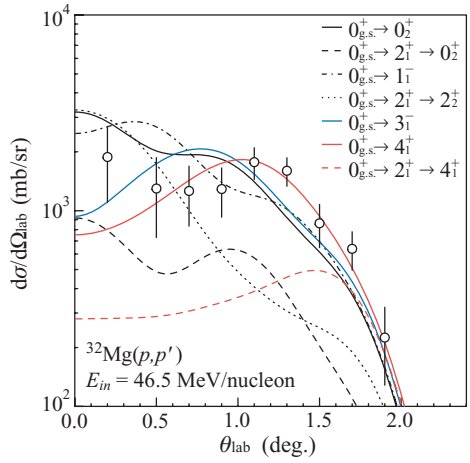

FIG. 6. (Color) Angular distributions for the excitation to the 2321-keV states in ^{32}Mg. The black curves show the calculations with $J^\pi = 0^+, 1^-$, and 2^+ assumed. The blue and red curves show the calculations for $J^\pi = 3^-$ and 4^+, respectively. For details see the text.

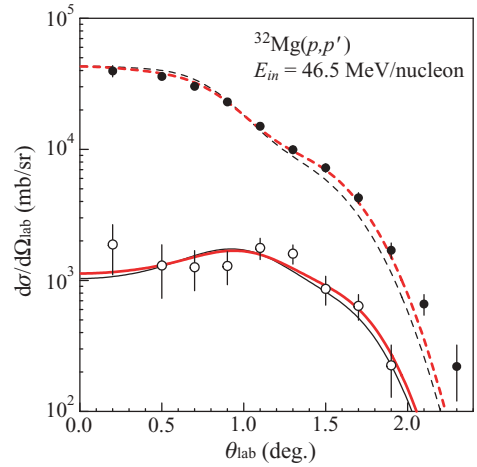

FIG. 7. (Color online) Angular distributions for the excitation to the 885- and 2321-keV states in ^{32}Mg, indicated by the closed and open circles. The red (thick) dashed and solid curves show the coupled-channel calculations for the 885- and 2321-keV states, respectively, with the KD02 potential. The black curves show the coupled-channel calculations with the CH89 potential.

with $J^\pi = 0^+, 1^-, 2^+$, and 3^- do not have a peaklike structure around 1.1°. To evaluate the agreements, the reduced-χ^2 values were obtained for different J^π. As seen in Table II, the reduced-χ^2 values for $J^\pi = 0^+$, 1^-, and 2^+ are larger than those for $J^\pi = 3^-$ and 4^+, which were found to be 1.9 and 0.6, respectively. Given the better χ^2 and agreement of the peak position, the $\Delta L = 4$ excitation or the 4^+ assignment is favored for the 2321-keV state.

To analyze the angular distribution in more detail, we combined the two-step rotational model ($0^+_{\text{g.s.}} \rightarrow 2^+_1 \rightarrow 4^+_1$) with the one-step excitation ($0^+_{\text{g.s.}} \rightarrow 4^+_1$). In this analysis, the adopted β_2 values were set to be the same for the $0^+_{\text{g.s.}} \rightarrow 2^+_1$ and $2^+_1 \rightarrow 4^+_1$ excitations. The β_2 and β_4 parameters are obtained to be 0.428(27) and 0.118(13), respectively, by the best fits with the KD02 potential. The results are shown in Fig. 7. The solid and dashed red curves show the calculated distributions for the 2321-keV and the 2^+_1 states, respectively. In the case of the calculations using CH89 (the black curves in Fig. 7), the β_2 and β_4 parameters are deduced to be 0.474(29) and 0.126(15), respectively. Both calculations well reproduce the experimental angular distribution, and the reduced-χ^2 values are 0.6 and 0.8 with the potentials KD02 and CH89, respectively. These results further support the $\Delta L = 4$ nature of the transition to the 2321-keV state. Therefore, we assign $J^\pi = 4^+$ to the 2321-keV state.

2. *Excited states above 2321 keV*

Angular distributions for excitations to several levels above the 2321-keV state were also obtained as shown in Fig. 8. Dots with statistical error bars represent experimental data. For simplicity, one-phonon excitations in the vibrational model were assumed in the ECIS97 calculations. In Fig. 8, the solid, dashed, dot-dashed, and dotted curves represent the results

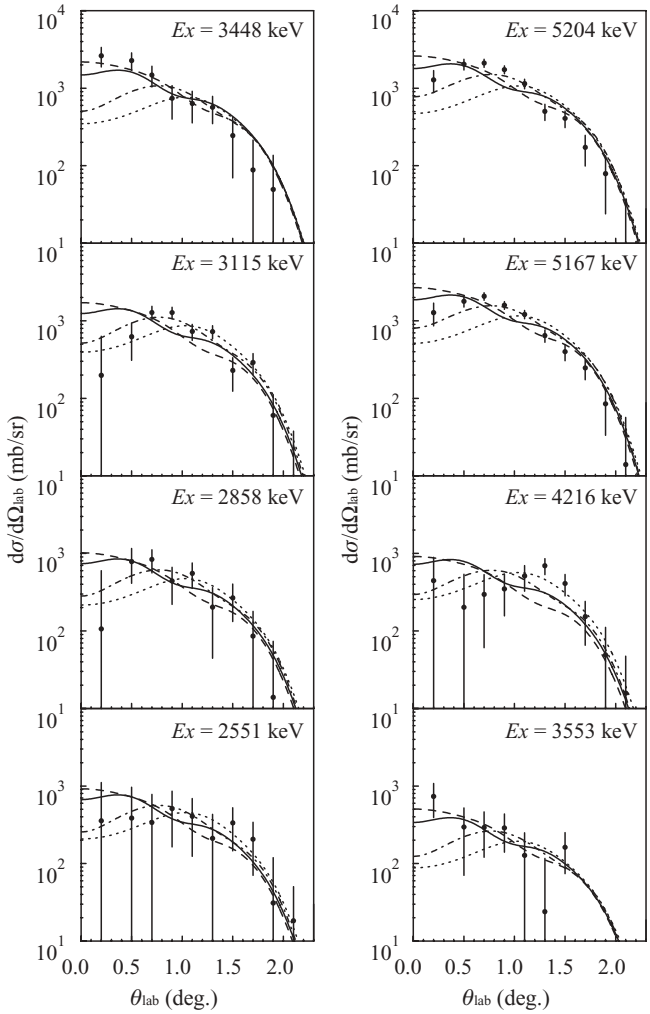

FIG. 8. Angular distributions for the excitation to states higher than the 2321-keV state in the ^{32}Mg(p, p') reaction. The solid, dashed, dot-dashed, and dotted curves represent the harmonic vibrational model calculations with transferred angular momenta of 1, 2, 3, and 4, respectively.

of the calculations with $\Delta L = 1, 2, 3$, and 4, respectively, assumed using the KD02 potential. In the calculations, each curve is normalized to the experimental angular distribution by adjusting the amplitude parameter β_λ.

Among the eight cases shown in Fig. 8, the distribution for the excitation to the 3448-keV state exhibits a clear forward-peaking pattern. It is consistent with $\Delta L = 1$ or $\Delta L = 2$, whereas the calculations with $\Delta L = 3$ and $\Delta L = 4$ do not reproduce the data as seen in the figure. The angular distributions for the 3115-, 5167-, and 5204-keV states, with relatively large cross sections (see Table. I), are similar to each other. The peaks of these distributions are located around 0.7°, which is consistent with $\Delta L = 3$ calculations, as indicated by the dot-dashed curves. The candidates of ΔL obtained by χ^2 analyses are listed in Table III with the corresponding amplitude parameters. The 2551- and 3553-keV states are not listed, because the determination of ΔL is ambiguous because of a lack of statistics. In the present study, the observed excited

TABLE III. Excitation energies, transferred angular momenta, and amplitudes.

E_x (keV)	ΔL	β_λ
2858	1, 3	$\beta_1 = 0.061$, $\beta_3 = 0.076$
3115	3, 4	$\beta_3 = 0.102$, $\beta_4 = 0.109$
3488	1, 2	$\beta_1 = 0.087$, $\beta_2 = 0.097$
4216	3, 4	$\beta_3 = 0.076$, $\beta_4 = 0.089$
5167	2, 3	$\beta_2 = 0.110$, $\beta_3 = 0.124$
5204	2, 3	$\beta_2 = 0.109$, $\beta_3 = 0.122$

states are assumed to be of natural parity. Unnatural-parity states may also be excited by proton inelastic scattering usually with lower cross sections.

Given the peak positions and the behavior at forward angles seen in the experimental angular distributions, assignments of $\Delta L = 3$ are reasonable for the 3115-, 5167-, and 5204-keV states. Corresponding $B(E3)$ values can be extracted from the β_3 values obtained in the χ^2 analysis. As described in Ref. [62], the $B(E3)$ values evaluated from the β_3 value obtained in the proton inelastic scattering are in substantial agreement with those determined by the more traditional methods, such as Coulomb excitation or lifetime measurement. The $B(E3)$ values for the 3115-, 5167-, and 5204-keV states are obtained to be 0.6, 0.9, and 0.9 W.u., respectively, suggesting a single-particle character of these states. On the basis of the 3^- assumption, the 3115-keV state with its small $B(E3)$ value together with the relatively low excitation energy may be an indication of the vanishing of the $N = 20$ shell gap in ^{32}Mg as discussed in Sec. I.

In the angular distribution of the 4216-keV state, the peak position is at a higher angle, around 1.3°, even larger than the peak angle expected for $\Delta L = 4$, implying J^π higher than 4^+, such as 6^+, but the χ^2 analysis favors $\Delta L = 3$ and $\Delta L = 4$ (see Table III). The location of the 6^+ state estimated by systematics for the ground-state bands of even-even nuclei [63] is 4.3 MeV, which is close to 4216 keV.

C. Two-neutron removal reaction of ^{32}Mg

In addition to the inelastic channel, the two-neutron removal reaction was studied simultaneously. Figure 9 shows the γ-ray spectrum measured in coincidence with the reaction product ^{30}Mg detected and identified by the TOMBEE system. The prominent γ line at $E_\gamma = 1482$ keV corresponds to the transition from the 2_1^+ state to the ground state. The peak at about 1900 keV has a width that is larger than the experimental resolution, suggesting that the peak is composed of at least two separate γ lines. The solid curve shows the result of the fit using the response functions for the known 1482-, 1820-, and 1947-keV γ rays [31,64,65]. The 1820-keV line corresponds to the transition from the 3302-keV state to the 2_1^+ state [64]; the 1947-keV transition is the one from the 4415-keV state with $J^\pi = (1, 2^+)$ [66] to the 2468-keV state with $J^\pi = (2^+)$ [64], as reported in Ref. [65].

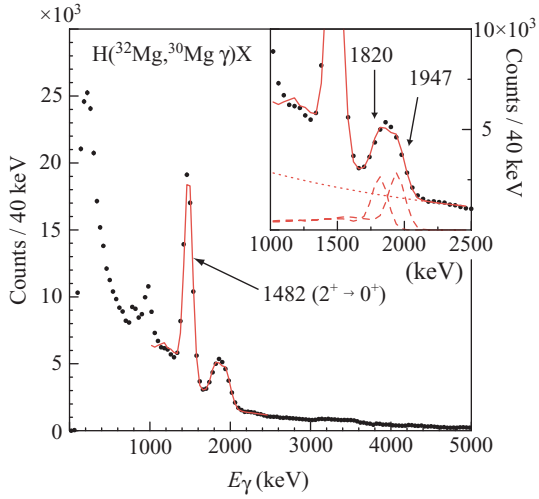

FIG. 9. (Color online) Doppler-corrected γ-ray spectra obtained in the two-neutron removal reaction on ^{32}Mg. The inset shows an expanded spectrum in the energy region from 1000 to 2500 keV. The red solid curve shows the fitting result using the response functions (dashed curves) and the exponential curve (dotted curve).

For the 3302-keV state, however, the spin and parity were not constrained in the β-decay studies [31,65] or in the study of β-delayed neutron emission from ^{31}Na [64]. It is known that the yrast states are preferentially observed in fragmentation-like reactions. For example, the 4^+ states were observed with large cross sections in the ^{36}S + ^{9}Be [67] and ^{36}Si + ^{9}Be [54] fragmentation reactions, as well as in the two-proton knockout reaction on ^{32}Mg [68]. Therefore, we conclude that J^π of the 3302-keV state is most probably 4^+.

IV. DISCUSSION

A. Proton and neutron contributions in the 2^+ excitation

Since proton scattering is sensitive to both proton and neutron excitations, the β_2 value obtained in the ^{32}Mg(p, p') experiment can be used to separate the neutron and proton contributions in the 2^+ excitation by comparing it with the deformation parameter deduced from the $B(E2)$ value determined by Coulomb excitation experiments.

According to the systematic study by Bernstein, Brown, and Madsen [34,35], the ratio of the neutron and proton matrix elements is expressed as

$$\frac{M_n}{M_p} = \frac{b_p}{b_n}\left[\frac{\delta^{p,p'}}{\delta^{\rm em}}\left(1+\frac{b_n}{b_p}\frac{N}{Z}\right)-1\right], \qquad (1)$$

where $M_{n(p)}$ denotes the neutron (proton) matrix element, $\delta^{p,p'}$ and $\delta^{\rm em}$ are the deformation lengths from (p, p') and Coulomb excitation, respectively, and b_n/b_p is the ratio of the sensitivity parameters for the neutron and the proton, which is approximately 3 in the present energy regime [34]. The deformation lengths and resultant M_n/M_p ratios obtained by using Eq. (1) are listed in Table IV.

TABLE IV. Deformation lengths and experimental M_n/M_p ratios for the excitation to the first 2^+ state in ^{32}Mg. The deformation length $\delta^{\rm em}$ is taken to be 1.95(17) fm [3].

	$\delta^{p,p'}$ (fm)	M_n/M_p	$\left(\frac{M_n}{M_p}\right)/\left(\frac{N}{Z}\right)$
KD02	1.60(10)	1.31(18)	0.78(11)
CH89	1.77(11)	1.49(19)	0.89(12)

The $B(E2)$ value of 454(78) e^2 fm^4 [3] is adopted in this study.[1] The corresponding deformation length $\delta^{\rm em}$ is obtained to be 1.95(17) fm by using the relation $\delta^{\rm em} = \beta_2^{\rm em} R$, where $R = 1.2A^{1/3}$ fm. For $\delta^{p,p'}$, analyses with the two optical potential parameter sets, KD02 and CH89, give an average value of $1.69^{+0.20}_{-0.19}$ fm. The M_n/M_p ratio divided by the proton-neutron ratio N/Z is thus obtained to be 0.84(15). As discussed by Bernstein, Brown, and Madsen [34,35], the double ratio $(\frac{M_n}{M_p})/(\frac{N}{Z})$ is close to unity, as in the present case for ^{32}Mg (0.84), when the collectivity of neutrons is as large as that of protons. This result for M_n/M_p for the 2^+ excitation in ^{32}Mg indicates that neutrons with the magic number $N = 20$ behave similarly to protons that fill partly the sd-shell orbital and thus provides additional evidence for the vanishing of the $N = 20$ shell gap in ^{32}Mg, which has been suggested by the low $E_x(2_1^+)$ and large $B(E2)$ values [2,3].

To examine this analysis with the global optical potentials and macroscopic coupling potential, microscopic calculations were performed. The proton-nucleus optical potential was obtained by folding the effective nucleon-nucleon interaction with the proton and neutron densities. The JLM potential proposed by Jeukenne, Lejeune, and Mahaux [69] was adopted for the nucleon-nucleon interaction. The normalization factors λ_v and λ_w were introduced for the real and imaginary parts of the JLM potential, respectively, which will be discussed later. The effective range parameter was assumed to be 1.2 fm as in Ref. [44]. The proton and neutron densities were assumed to have the same root-mean-square (rms) radius and were obtained by the systematics proposed by Negele [70]. The transition densities were obtained by differentiating the proton and neutron densities and were folded with the JLM potential to deduce coupling potentials. The amplitudes of the proton and neutron transition densities are related to the proton- and neutron-deformation lengths (δ_p and δ_n), respectively, the former of which is fixed to be consistent with the adopted $B(E2)$ value whereas the latter is treated as a adjustable parameter. The MINC [71] code was used for reduction of the potentials by the procedure described earlier.

[1] Among $B(E2)$ values reported in other studies, the ones in Refs. [5,8] are in good agreement with the value adopted here. In Refs. [4,7], lower $B(E2)$ values are extracted by correcting for feeding from the 2321-keV state by assuming its spin of 1^-, 1^+, or 2^+ rather than 4^+. Since 4^+ states are populated only weakly in intermediate-energy Coulomb excitation, the expected feeding correction should be much smaller, and the experimental cross sections in Refs. [4,7] should become consistent with the $B(E2)$ value adopted in the present analysis, if $J^\pi = 4^+$ is assumed for the 2321-keV state.

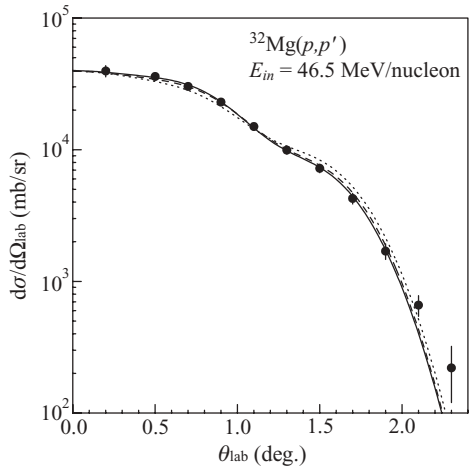

FIG. 10. Distributions calculated by microscopic analyses with the JLM potential for excitation to the first 2^+ state. The solid, dashed, and dotted curves show the calculations with parameter sets a, b, and c, respectively, which are listed in Table V.

Results of coupled-channel calculations for the 2_1^+ excitation using ECIS97 are shown in Fig. 10, together with the experimental angular distribution. Solid, dashed, and dotted curves show the calculated distributions with parameter sets a, b, and c listed in Table V, respectively. The parameter R is the rms radius of the density distribution. The value 3.26 fm in a and c is obtained from the density distribution proposed by Negele [70], whereas 3.12 fm in b is reported by Suzuki *et al.* [72] based on the interaction cross-section measurement. The normalization factors $\lambda_v = \lambda_w = 0.95$ in a and b are taken from Ref. [44], in which the factors were obtained by analyzing proton elastic scattering on ^{32}S with the same mass number as ^{32}Mg. The set $\lambda_v = 1.00$ and $\lambda_w = 0.80$ is the one frequently adopted. As discussed before, the proton deformation length δ_p was calculated from the adopted $B(E2)$ value and the parameter R, and the neutron deformation length δ_n was adjusted so as to reproduce the experimental angular distribution by the ECIS97 calculation. All curves reproduce the measured distribution well, though the deviation of the calculation with parameter set c from the measured distribution is relatively large compared with the other calculated curves. It should be noted that the double ratio $(\frac{M_n}{M_p})/(\frac{N}{Z})$ is directly obtained by the ratio δ_n/δ_p.

The $(\frac{M_n}{M_p})/(\frac{N}{Z})$ value obtained by averaging over the three cases is $0.94^{+0.28}_{-0.20}$, which agrees within the errors with 0.84(15)

TABLE V. The rms radii, normalization factors, deduced deformation lengths, and $(\frac{M_n}{M_p})/(\frac{N}{Z})$ values.

	R (fm)	λ_v	λ_w	δ_p (fm)	δ_n (fm)	$(\frac{M_n}{M_p})/(\frac{N}{Z})$
a	3.26	0.95	0.95	$1.82^{+0.15}_{-0.16}$	$1.88^{+0.15}_{-0.14}$	$1.03^{+0.19}_{-0.15}$
b	3.12	0.95	0.95	$1.91^{+0.16}_{-0.17}$	$1.77^{+0.14}_{-0.13}$	$0.93^{+0.17}_{-0.13}$
c	3.26	1.00	0.80	$1.82^{+0.15}_{-0.16}$	$1.59^{+0.12}_{-0.14}$	$0.87^{+0.16}_{-0.13}$

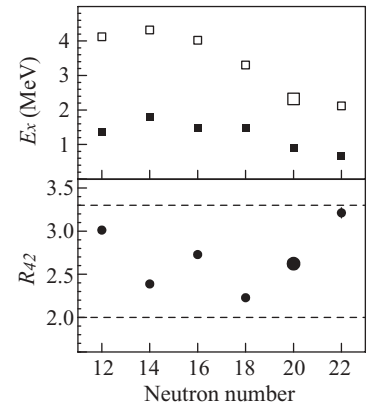

FIG. 11. (Top) Excitation energies for 2_1^+ and 4_1^+ states, indicated by closed and open squares, respectively. (Bottom) Ratio between the energies of the 2_1^+ and 4_1^+ states (R_{42}) for Mg isotopes. The dashed lines indicate the vibrational and rigid-rotor limits for R_{42}.

extracted in the analysis using the global optical potentials with Bernstein's method with the help of Eq. (1). Thus the conclusion on the vanishing of the $N = 20$ shell gap is further supported by the microscopic analysis that includes automatically the sensitivity of the (p, p') reaction to neutron and proton excitations through the JLM effective interaction.

B. Nature of collectivity in ^{32}Mg

Figure 11 shows plots of $E_x(2_1^+)$, $E_x(4_1^+)$, and R_{42} for the neutron-rich Mg isotopes, where R_{42} is the ratio between the energies of the 4_1^+ and 2_1^+ states. The 4_1^+ energies for ^{30}Mg and ^{32}Mg are from the present study (see Sec. III). The ratio R_{42} is close to the vibration limit 2.0 for ^{30}Mg as expected for nuclei close to the shell closure, whereas the ratio takes a larger value, 2.6, for ^{32}Mg, reflecting the disappearance of the sd-pf shell gap in this nucleus. For ^{34}Mg with $N = 22$, the nature of collectivity is almost the one expected for a rigid rotor, since the R_{42} value approaches the limit 3.3. The value 2.6 for ^{32}Mg lies in between the two limits, indicating a "transitional" nature of the collectivity. The development of collectivity from ^{30}Mg through ^{32}Mg toward ^{34}Mg seen in Fig. 11 is consistent with the behavior of their $B(E2)$ values, increasing from ^{30}Mg to ^{34}Mg.

V. SUMMARY

Excited states in the neutron-rich nucleus ^{32}Mg were studied by proton inelastic scattering in inverse kinematics via an in-beam γ-ray spectroscopy technique. A level scheme, including five new states, was constructed by using γ-γ coincidence analyses. The differential cross sections were analyzed by using coupled-channel calculations to determine the transferred angular momenta and the amplitudes of individual transitions. In this study, J^π of the 2321-keV state was assigned for the first time as 4_1^+; several different assignments have been previously reported. The R_{42} ratio of 2.6 is in between the vibrational and rigid-rotor limits. The

systematic behavior of R_{42} in the Mg isotopes suggests a development of deformation in ^{32}Mg starting from spherical ^{30}Mg toward well-deformed ^{34}Mg. A candidate for the 3_1^- state was found at an excitation energy of 3115 keV, which is lower than the 3_1^- energies in other $N = 20$ isotones. A small $B(E3)$ value of 0.6 W.u. suggests a single-particle nature. For the excitation from the ground state to the 2_1^+ state, the deformation length $\delta^{p,p'}$ was obtained to be $1.69\ ^{+0.20}_{-0.19}$ fm. The $(\frac{M_n}{M_p})/(\frac{N}{Z})$ ratio was deduced to be 0.84(15) by combining $\delta^{p,p'}$ with the known $B(E2)$ value. This was supported by a microscopic analysis using the JLM potential. These results all together support the picture of a vanishing $N = 20$ magic number in ^{32}Mg. Moreover, they might give deeper insights into the mechanism for the emergence of the island of inversion through further theoretical studies.

ACKNOWLEDGMENTS

We would like to thank the RIKEN Ring Cyclotron staff members for their operation during the experiment. We are grateful to Dr. D. Steppenbeck for proofreading of this article. Construction of DALI2 was partially supported by Research Center for Measurement in Advanced Science at Rikkyo University. One of the authors (ST) is grateful for the support of the Special Postdoctoral Researcher Program at RIKEN.

[1] E. K. Warburton, J. A. Becker, and B. A. Brown, Phys. Rev. C **41**, 1147 (1990).
[2] C. Détraz, D. Guillemaud, G. Huber, R. Klapisch, M. Langevin, F. Naulin, C. Thibault, L. C. Carraz, and F. Touchard, Phys. Rev. C **19**, 164 (1979).
[3] T. Motobayashi *et al.*, Phys. Lett. **B346**, 9 (1995).
[4] B. V. Pritychenko *et al.*, Phys. Lett. **B461**, 322 (1999).
[5] H. Iwasaki *et al.*, Phys. Lett. **B522**, 227 (2001).
[6] V. Chisté *et al.*, Phys. Lett. **B514**, 233 (2001).
[7] J. A. Church *et al.*, Phys. Rev. C **72**, 054320 (2005).
[8] O. T. Niedermaier, Ph.D. thesis, the Ruperto-Carola University of Heidelberg, 2005, http://www.ub.uni-heidelberg.de/archiv/5647/.
[9] A. Navin *et al.*, Phys. Rev. Lett. **85**, 266 (2000).
[10] H. Iwasaki *et al.*, Phys. Lett. **B481**, 7 (2000).
[11] H. Iwasaki *et al.*, Phys. Lett. **B491**, 8 (2000).
[12] S. Shimoura *et al.*, Phys. Lett. **B560**, 31 (2003).
[13] O. Sorlin *et al.*, Phys. Rev. C **47**, 2941 (1993).
[14] H. Scheit *et al.*, Phys. Rev. Lett. **77**, 3967 (1996).
[15] A. Ozawa, T. Kobayashi, T. Suzuki, K. Yoshida, and I. Tanihata, Phys. Rev. Lett. **84**, 5493 (2000).
[16] A. Poves and J. Retamosa, Phys. Lett. **B184**, 311 (1987).
[17] N. Fukunishi, T. Otsuka, and T. Sebe, Phys. Lett. **B296**, 279 (1992).
[18] T. Otsuka and N. Fukunishi, Phys. Rep. **264**, 297 (1996).
[19] Y. Utsuno, T. Otsuka, T. Mizusaki, and M. Honma, Phys. Rev. C **60**, 054315 (1999).
[20] E. Caurier, F. Nowacki, A. Poves, and J. Retamosa, Phys. Rev. C **58**, 2033 (1998).
[21] E. Caurier, F. Nowacki, and A. Poves, Nucl. Phys. **A693**, 374 (2001).
[22] J. Terasaki, H. Flocard, P.-H. Heenen, and P. Bonche, Nucl. Phys. **A621**, 706 (1997).
[23] P.-G. Reinhard, D. J. Dean, W. Nazarewicz, J. Dobaczewski, J. A. Maruhn, and M. R. Strayer, Phys. Rev. C **60**, 014316 (1999).
[24] M. Yamagami and N. Van Giai, Phys. Rev. C **69**, 034301 (2004).
[25] R. Rodríguez-Guzmán, J. L. Egido, and L. M. Robledo, Phys. Lett. **B474**, 15 (2000).
[26] S. Péru, M. Girod, and J. F. Berger, Eur. Phys. J. A **9**, 35 (2000).
[27] W. Mittig *et al.*, Eur. Phys. J. A **15**, 157 (2002).
[28] V. Tripathi *et al.*, Phys. Rev. C **77**, 034310 (2008).
[29] F. Azaiez *et al.*, Eur. Phys. J. A **15**, 93 (2002).
[30] D. Guillemaud-Mueller, Eur. Phys. J. A **13**, 63 (2002).
[31] D. Guillemaud-Mueller, C. Detraz, M. Langevin, F. Naulin, M. D. Saint-Simon, C. Thibault, F. Touchard, and M. Epherre, Nucl. Phys. **A426**, 37 (1984).
[32] G. Klotz, P. Baumann, M. Bounajma, A. Huck, A. Knipper, G. Walter, G. Marguier, C. Richard-Serre, A. Poves, and J. Retamosa, Phys. Rev. C **47**, 2502 (1993).
[33] C. M. Mattoon *et al.*, Phys. Rev. C **75**, 017302 (2007).
[34] A. M. Bernstein, V. R. Brown, and V. A. Madsen, Phys. Lett. **B103**, 255 (1981).
[35] A. M. Bernstein *et al.*, Comments Nucl. Part. Phys. **11**, 203 (1983).
[36] Y. Yanagisawa *et al.*, Phys. Lett. **B566**, 84 (2003).
[37] L. A. Riley *et al.*, Phys. Rev. C **72**, 024311 (2005).
[38] H. J. Ong *et al.*, Phys. Rev. C **73**, 024610 (2006).
[39] C. M. Campbell *et al.*, Phys. Lett. **B652**, 169 (2007).
[40] N. Aoi *et al.*, Phys. Rev. Lett. **102**, 012502 (2009).
[41] Z. Elekes *et al.*, Phys. Lett. **B599**, 17 (2004).
[42] G. Kraus *et al.*, Phys. Rev. Lett. **73**, 1773 (1994).
[43] J. H. Kelley *et al.*, Phys. Rev. C **56**, R1206 (1997).
[44] F. Maréchal *et al.*, Phys. Rev. C **60**, 034615 (1999).
[45] D. Gupta and D. N. Basu, Nucl. Phys. **A748**, 402 (2005).
[46] D. Gupta, E. Khan, and Y. Blumenfeld, Nucl. Phys. **A773**, 230 (2006).
[47] C. M. Campbell *et al.*, Phys. Rev. Lett. **97**, 112501 (2006).
[48] T. Kubo, M. Ishihara, N. Inabe, H. Kumagai, I. Tanihata, K. Yoshida, T. Nakamura, H. Okuno, S. Shimoura, and K. Asahi, Nucl. Instrum. Methods Phys. Res. B **70**, 309 (1992).
[49] H. Kumagai, A. Ozawa, N. Fukuda, K. Summerer, and I. Tanihata, Nucl. Instrum. Methods Phys. Res. A **470**, 562 (2001).
[50] H. Ryuto, M. Kunibu, T. Minemura, T. Motobayashi, K. Sagara, S. Shimoura, M. Tamaki, Y. Yanagisawa, and Y. Yano, Nucl. Instrum. Methods Phys. Res. A **555**, 1 (2005).
[51] N. Aoi *et al.*, RIKEN Accel. Prog. Rep. **38**, 176 (2005).
[52] K. Kusaka, T. Kubo, Y. Mizoi, K. Yoshida, A. Yoshida, T. Tominaka, Y. Yano, T. Tsuchihashi, N. Kakutani, and K. Sato, IEEE Trans. Appl. Supercond. **14**, 310 (2004).
[53] M. Tamaki *et al.*, CNS-REP **59**, 76 (2003).
[54] K. Yoneda *et al.*, Phys. Lett. **B499**, 233 (2001).
[55] S. Takeuchi *et al.*, RIKEN Accel. Prog. Rep. **36**, 148 (2003).
[56] GEANT3, CERN Program Library Long Writeup W5013, http://wwwasdoc.web.cern.ch/wwwasdoc/geant_html3/geantall.html.
[57] G. F. Knoll, *Radiation Detection and Measurement* (Wiley, New York, 1979), and references therein.

[58] W. R. Leo, *Techniques for Nuclear and Particle Physics Experiments* (Springer-Verlag, Berlin, 1994), and references therein.
[59] J. Raynal, coupled-channel code ECIS97 (unpublished).
[60] A. J. Koning and J. P. Delaroche, Nucl. Phys. **A713**, 231 (2003).
[61] R. L. Varner, W. J. Thompson, T. L. McAbee, E. J. Ludwig, and T. B. Clegg, Phys. Rep. **201**, 57 (1991).
[62] T. Kibédi and R. H. Spear, At. Data Nucl. Data Tables **80**, 35 (2002).
[63] D. Bucurescu, N. V. Zamfir, G. Căta-Danil, M. Ivaşcu, and N. Mărginean, Phys. Rev. C **78**, 044322 (2008), and references therein.
[64] H. Mach *et al.*, Eur. Phys. J. A **25**, s1.105 (2005).
[65] P. Baumann *et al.*, Phys. Rev. C **39**, 626 (1989).
[66] NNDC data base ENSDF, http://www.nndc.bnl.gov/ensdf.
[67] M. Belleguic *et al.*, Phys. Scr. **T88**, 122 (2000).
[68] P. Fallon *et al.*, J. Phys.: Conf. Ser. **49**, 165 (2006).
[69] J.-P. Jeukenne, A. Lejeune, and C. Mahaux, Phys. Rev. C **16**, 80 (1977).
[70] J. W. Negele, Phys. Rev. C **1**, 1260 (1970).
[71] M. Takashina, single-folding code MINC (unpublished).
[72] T. Suzuki *et al.*, Nucl. Phys. **A630**, 661 (1998).